

Anomalous transverse response of Co₂MnGa and universality of the room-temperature $\alpha_{ij}^A/\sigma_{ij}^A$ ratio across topological magnets

Liangcai Xu^{1,2}, Xiaokang Li^{1,2}, Linchao Ding¹, Taishi Chen^{3,4,5}, Akito Sakai^{3,4,5},
Benoît Fauqué⁶, Satoru Nakatsuji^{3,4,5}, Zengwei Zhu^{1,*} and Kamran Behnia^{2,*}

(1) Wuhan National High Magnetic Field Center and School of Physics,
Huazhong University of Science and Technology,
Wuhan 430074, China

(2) Laboratoire de Physique Et Etude des Matériaux (UPMC-CNRS),
ESPCI Paris, PSL Research University, 75005 Paris, France

(3) Institute for Solid State Physics,
University of Tokyo, Kashiwa, Chiba 277-8581, Japan

(4) Department of Physics, University of Tokyo,
Hongo, Bunkyo-ku, Tokyo 113-0033, Japan

(5) CREST, Japan Science and Technology Agency (JST),
4-1-8 Honcho Kawaguchi, Saitama 332-0012, Japan

(6) Collège de France,
11 place Marcelin Berthelot, 75005 Paris, France

(Dated: March 8, 2024)

The off-diagonal (electric, thermal and thermoelectric) transport coefficients of a solid can acquire an anomalous component due to the non-trivial topology of the Bloch waves. We present a study of the anomalous Hall (AHE), Nernst (ANE) and thermal Hall effects (ATHE) in the Heusler Weyl ferromagnet Co₂MnGa. The Anomalous Wiedemann-Franz law, linking electric and thermal responses, was found to be valid over the whole temperature window. This indicates that the AHE has an intrinsic origin and the Berry spectrum is smooth in the immediate vicinity of the Fermi level. From the ANE data, we extract the magnitude and temperature dependence of α_{ij}^A and put under scrutiny the $\alpha_{ij}^A/\sigma_{ij}^A$ ratio, which approaches k_B/e at room temperature. We show that in various topological magnets the room-temperature magnitude of this ratio is a sizeable fraction of k_B/e and argue that the two anomalous transverse coefficients depend on universal constants, the Berry curvature averaged over a window set by either the Fermi wavelength (for Hall) or the de Broglie thermal length (for Nernst). Since the ratio of the latter two is close to unity at room temperature, such a universal scaling finds a natural explanation in the intrinsic picture of anomalous transverse coefficients.

The anomalous Hall effect (AHE)¹⁻³ has thermoelectric and thermal counterparts, which emerge whenever the longitudinal electric field is replaced by a longitudinal temperature gradient. When intrinsic, the anomalous Nernst (ANE) and the anomalous Righi-Leduc (or thermal Hall (ATHE) effects, like AHE, are caused by the non-vanishing Berry curvature of Bloch waves in the host solid⁴⁻⁸. A recent theme of interest is the magnitude of these anomalous coefficients. Universal scaling between the amplitudes of magnetization and the amplitude of the transverse response has been sought and invalidated^{4,7,9}. Correlations among anomalous transverse coefficients themselves has also been explored. The anomalous version of the Wiedemann-Franz law, establishing a link between the magnitude of AHE and ARLE has been tested^{6,10,11} and the validity of the Mott's relation linking AHE and ANE has been investigated^{6,7,12-14}.

In this paper, we present an extensive study of the three anomalous transport coefficients of Co₂MnGa and report on several new findings. First of all, we find that the anomalous Wiedemann-Franz law (WF) holds in this system between 2K and 300 K. To the best of our knowledge, this is the unique case of such an extensive verification. Second, we quantify α_{ij}^A and confirm that, as no-

ticed previously^{8,9}, α_{ij}^A is exceptionally large in this system. We quantify the temperature dependence of $\alpha_{ij}^A/\sigma_{ij}^A$ ratio and find that it tends to saturate to a sizeable fraction of k_B/e at high temperature. We then show that ratio of $\alpha_{ij}^A/\sigma_{ij}^A$ at room temperature in all known topological magnets lies between 0.2 k_B/e and 0.9 k_B/e in spite of a tenfold variation in the amplitude of α_{ij}^A . We will see below that such a striking correlation is expected when the anomalous transverse response is intrinsic. It implies that the large α_{ij}^A in this system^{8,9} is unsurprising given its large σ_{ij}^A .

Co₂MnGa is a Weyl ferromagnet^{8,15} with a Heusler L2₁ structure. It has a Curie temperature of $T_C \approx 694$ K and a saturation moment of 4 μ_B per formula unit¹⁶. Previous studies have reported on strain-induced magnetic anisotropy¹⁷ and negative anisotropic magnetoresistance¹⁸. Recently, a large anomalous Hall conductivity exceeding 1000 $\Omega \text{ cm}^{-1}$ has been observed in thin films and more 2000 $\Omega \text{ cm}^{-1}$ in crystals of Co₂MnGa^{8,19,20}. A large anomalous Nernst effect was also reported by a number of previous authors^{8,9,14,21}. The magnitude of room-temperature ANE in crystals was found to be remarkably large^{8,9}. Guin *et al.*⁹ reported that S_{xy}^A is much larger than what is expected according to a simple scal-

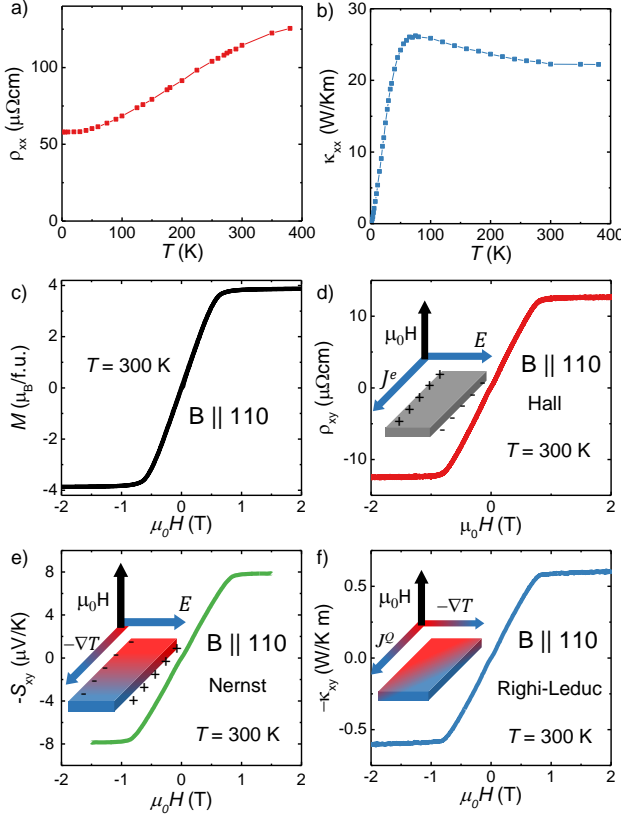


FIG. 1. **Basic transport and anomalous transverse responses at ($T = 300$ K) in Co_2MnGa :** Temperature dependence of electric (a) and thermal conductivity (b). (c) Magnetization M at room temperature. (d) Anomalous Hall effect (e) anomalous Nernst effect, and (f) anomalous thermal Hall effect at room temperature. In all cases in this paper, $B \parallel [110]$, $I \parallel [001]$. The insets in (d-f) show the experimental configurations for Hall, Nernst and thermal Hall measurements.

ing with magnetization and Sakai *et al.* invoked a quantum critical scaling for α_{xy}^A ⁸. In this context, and as we will see below, a comparison of the $\alpha_{ij}^A/\sigma_{ij}^A$ across various magnets is illuminating. Despite the fact that σ_{ij}^A varies hundredfold (8 to 1000 $\Omega^{-1}\text{cm}^{-1}$) in different topological magnets, the ratio of $\alpha_{ij}^A/\sigma_{ij}^A$ remains a sizeable fraction of k_B/e .

Figure 1(a) and (b) show the temperature dependence of the thermal conductivity, κ_{xx} and electric resistivity, ρ_{xx} . Resistivity varies from 125 $\mu\Omega\text{cm}$ at room temperature to 60 $\mu\Omega\text{cm}$ at low temperature. This implies a short mean-free-path for electrons and given the magnitude of κ_{xx} a dominant role for phonons (and eventually magnons) in longitudinal thermal transport.

As seen in Figure 1(c), room temperature magnetization saturates to 4 $\mu_B/\text{f.u.}$, similar to what was reported previously^{8,19}. In contrast to other topological magnets^{6,10,13}, no clear hysteresis loop is visible, indicating that the domain walls smoothly propagate with-

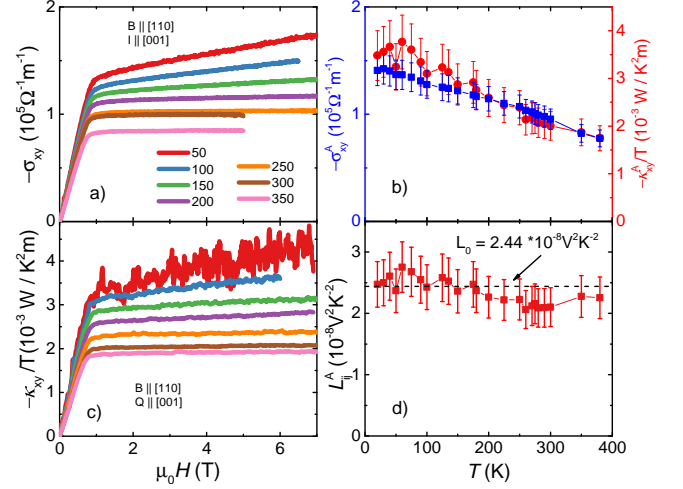


FIG. 2. **Temperature evolution of Hall conductivity and thermal Hall conductivity and Anomalous transverse Lorenz number in Co_2MnGa :** (a) and (b) Field dependent Hall conductivity σ_{xy} and transverse thermal conductivity divided by T κ_{xy}/T at selected temperatures. (c) Temperature dependent anomalous Hall conductivity and transverse thermal conductivity. (d) The anomalous transverse Lorenz ratio ($L_{xy}^A = \kappa_{xy}^A/\sigma_{xy}^A$).

out pinning when the magnetic field is swept. The field dependence of the Hall, Nernst and Righi-Leduc effects at room temperature are shown in Fig.1(d-f). They all display a behavior similar to the magnetization. The steep initial slope is replaced by a much smaller one at higher magnetic field. The anomalous component of the Hall resistivity ($\simeq 13\mu\Omega\text{cm}$) is slightly below what was previously reported ($\simeq 15\mu\Omega\text{cm}$)⁸ and the anomalous Nernst signal ($\simeq 8\mu\text{V/K}$) is somewhat larger than a previous report ($\simeq 6.5\mu\text{V/K}$)⁸. We note that the room-temperature anomalous S_{xy}^A in crystals^{8,9} is three to four times larger than in thin films^{14,21}.

Fig.2(a,c) shows the thermal evolution of the Hall conductivity (σ_{xy}) and the thermal Hall conductivity (κ_{xy}/T) in a field window extended to 7 T (The raw data can be seen in the supplement²²). In both cases, given the clear change in the slope of the curve, the extraction of the anomalous components is straightforward. Fig.2(b) shows how the anomalous Hall conductivity, σ_{xy}^A , and the anomalous thermal Hall conductivity κ_{xy}^A/T depend on temperature. Both increase almost twofold as the system is cooled from 300 K to 4 K. The validity of the anomalous WF law for transverse response can be checked by comparing the anomalous Lorenz number $L_{xy}^A = \frac{\kappa_{xy}^A}{T\sigma_{xy}^A}$

with the Sommerfeld value $L_0 = \frac{\pi^2}{3}(\frac{k_B}{e})^2$ where k_B and e are the Boltzmann constant and the elementary charge of electron. As seen in Fig.2(d), within experimental margin, we find that L remains close to L_0 and the anomalous WF law is verified.

In Fig.3(a), we compare the evolution of the anomalous Lorenz number L_{ij}^A in Co_2MnGa with those found in two other topological magnets. In the case of Mn_3Sn ⁶, the anomalous WF law was found to be held above 150 K. The commensurate triangular magnetic order is taken over by a helical one below this temperature. In Mn_3Ge ¹⁰, such a transition is absent and thus the validity of the anomalous WF law could be checked down to cryogenic temperatures, but a sizeable difference between L_{xy}^A and L_0 was observed above 100 K and attributed to a mismatch between thermal and electrical summations of the Berry curvature¹⁰. In common elemental ferromagnets, like Ni ²³ and Fe ⁶, L_{xy}^A was found to be close to L_0 at low temperature and a downward deviation emerges on heating, presumably due to inelastic scattering⁶. Thus, Co_2MnGa is the first case of a magnet in which the anomalous WF law remains valid between 4 K and 300 K. This means that not only inelastic scattering is irrelevant, but also the thermal and electrical summations of the Berry curvature match each other. Thus, the variation of the Berry curvature near the Fermi energy is not abrupt in contrast to the case of Mn_3Ge ¹⁰.

Fig.3(b) and (c) show the temperature dependence of σ_{xy}^A and α_{xy}^A . The magnitude of α_{xy}^A (which attains $1400 \text{ } \Omega \text{ cm}^{-1}$ at 2 K and decreases to $1000 \text{ } \Omega \text{ cm}^{-1}$ at room temperature) is remarkably large and in reasonable agreement with previous studies^{8,9}. The anomalous transverse thermoelectric conductivity, α_{xy}^A displays a non-monotonous temperature dependence decreasing only below 150 K and vanishing as expected in the zero-temperature limit. Our α_{xy}^A data is in reasonable agreement with Sakai and co-workers' data⁸, but does not match what was reported by Guin *et al.*⁹, discussed in the supplement²², this is due to an elementary mistake in manipulating the sign of the two components of α_{xy}^A . Rectifying this mistake, one finds that the three sets of data give comparable value at room-temperature²².

The low-temperature slope of α_{xy}^A can be quantified by plotting α_{xy}^A/T as a function of temperature²². According to the Mott's relation, this slope quantifies the variation of the low-temperature σ_{xy}^A caused by an infinitesimal shift in the chemical potential. The magnitude of the extracted slope in Co_2MnGa ($\alpha_{xy}^A/T \simeq -0.037 \text{ AK}^{-2} \text{ m}^{-1}$) is smaller than what was seen in $\text{Co}_3\text{Sn}_2\text{S}_2$ ¹³. In the latter case, the extracted slope was found to be in good agreement with the observed variation of low-temperature σ_{xy}^A caused by a small shift in the chemical potential¹³. Our data reveals a well-defined α_{xy}^A/T and merges to the $-\ln T$ behavior above 100 K, similarly to the one reported by a previous study⁸. (See the discussion in²²).

We now turn our attention to the magnitude of the $\alpha_{ij}^A/\sigma_{ij}^A$ ratio. In Fig.4a), we present the temperature dependence of this ratio in Co_2MnGa and compare it to the available data of other magnets. Among these five systems, $\text{Co}_3\text{Sn}_2\text{S}_2$ distinguishes itself by the sign

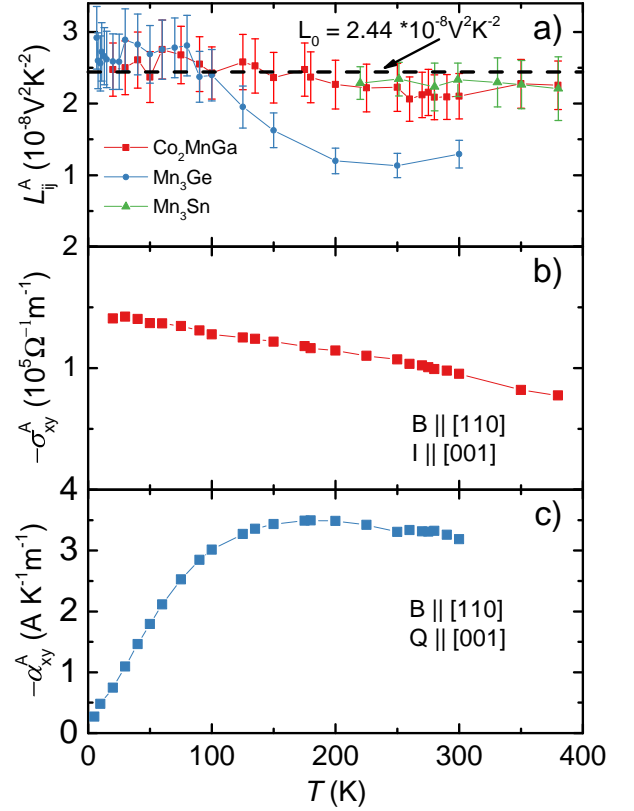


FIG. 3. **Anomalous Transverse coefficients:** (a) The anomalous Lorenz number $L_{xy}^A = \kappa_{xy}^A/T\sigma_{xy}^A$ remains close to the Sommerfeld value L_0 . The anomalous Lorenz number of Mn_3Sn ⁶ and Mn_3Ge ¹⁰ are also shown. The dashed horizontal line represents L_0 . (b) The anomalous Hall conductivity σ_{xy}^A as a function of temperature. (c) The anomalous transverse thermoelectric conductivity, α_{xy}^A , as a function of temperature. For comparison with data reported previously^{8,9}, see the supplement²².

change of α_{xy}^A around 60 K¹³. However, like the four other systems, this ratio tends towards saturation at a value which is a sizeable fraction of k_B/e .

As seen in Fig.4b), even though σ_{ij}^A changes by a factor of 100 among different magnetic materials, the room-temperature $\alpha_{ij}^A/\sigma_{ij}^A$ ratio remains between $k_B/5e$ and k_B/e , which is the natural units of the ratio of these two quantities. This observation begs an explanation within our present understanding of anomalous transverse coefficients caused by Berry curvature.

The following expressions link the anomalous Hall and the anomalous thermoelectric conductivity to the Berry curvature Ω^z

$$\sigma_{xy}^A = \frac{e^2}{\hbar} \int_{BZ} \frac{d^3k}{(2\pi)^3} f(k) \Omega^z \quad (1)$$

$$\alpha_{xy}^A = \frac{ek_B}{\hbar} \int_{BZ} \frac{d^3k}{(2\pi)^3} s(k) \Omega^z \quad (2)$$

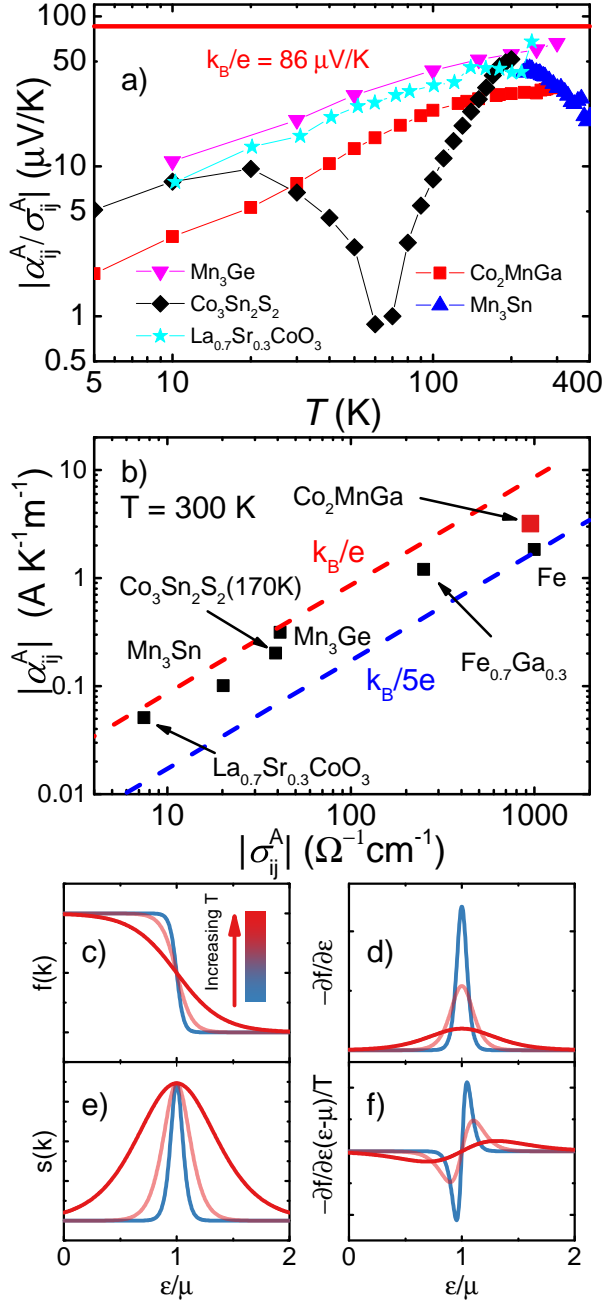


FIG. 4. **The universal relation found in $\alpha_{ij}^A/\sigma_{ij}^A$ ratio and the pondering functions:** a): The $\alpha_{ij}^A/\sigma_{ij}^A$ ratio as a function of temperature in different magnets including Mn_3Sn ⁶, Fe ⁶, Mn_3Ge ¹⁰, $\text{La}_{0.7}\text{Sr}_{0.3}\text{CoO}_3$ ²⁴ and $\text{Co}_3\text{Sn}_2\text{S}_2$ ¹³. k_B/e is represented by a red solid line. b): Room-temperature $\alpha_{ij}^A/\sigma_{ij}^A$ in different magnets ($\text{Fe}_{0.7}\text{Ge}_{0.3}$ ²⁵). All the points are shown at 300 K ($\text{Co}_3\text{Sn}_2\text{S}_2$ is taken at 170 K because of the magnetic order). They lie all between $k_B/5e$ (blue line) and k_B/e (red line). Note the range of σ^A between $8 \Omega^{-1}\text{cm}^{-1}$ and $1000 \Omega^{-1}\text{cm}^{-1}$. c-f) Pondering functions in Fermi sea (c and e) and Fermi surface (d and f) expressions of the anomalous Hall coefficients. c) Fermi-Dirac distribution, $f(k)$, used for Fermi-sea σ_{ij}^A . d) Its energy derivative, used for Fermi-surface σ_{ij}^A . e) The entropy density of electrons, $s(k)$, used for Fermi-sea α_{ij}^A . f) Its energy derivative, used for Fermi-surface α_{ij}^A .

Here $f(k)$ is the Fermi-Dirac distribution and $s(k) = -f(k)\ln(f(k)) - (1-f(k))\ln(1-f(k))$ is the (von Neuman) entropy density of electron gas, which are plotted in Fig.4c and Fig.4e. These 'Fermi sea' expressions for σ_{xy}^A and α_{xy}^A have 'Fermi surface' counterparts where the pondering factors are $\partial f/\partial \epsilon$ and $\partial s/\partial \epsilon = \frac{\partial f}{\partial \epsilon} \frac{(\epsilon - \mu)}{k_B T}$ (See the supplement for a discussion on the equivalency between the two formalisms).

Eq.1 implies that the anomalous Hall conductivity is an average of the Berry curvature over the occupied fermionic states. One can express this idea by writing¹³: $\sigma_{xy}^A \approx \frac{e^2}{h} \frac{1}{c} < \frac{\Omega_B}{\lambda_F^2} >$, where λ_F is the Fermi wavelength in the plane perpendicular to the magnetic field and c is the lattice parameter along the magnetic field. In contrast, Eq.2 implies that α_{xy}^A averages the Berry curvature over the states, which have a finite entropy, which within a thermal thickness of the Fermi level. Therefore $\alpha_{xy}^A \approx \frac{ek_B}{h} \frac{1}{c} < \frac{\Omega_B}{\Lambda^2} >$ ¹³, where $\Lambda = \sqrt{\frac{h^2}{2\pi m k_B T}}$ is the de Broglie thermal wavelength in the plane perpendicular to the magnetic field. According to these expressions, α_{xy}^A vanishes in the low temperature limit, because Λ will diverge. On the other hand, λ_F and therefore σ_{xy}^A are expected to be finite in the whole temperature range. Now, the $\alpha_{xy}^A/\sigma_{xy}^A$ will be set by $\frac{k_B}{e} < \frac{\lambda_F^2}{\Lambda^2} >$. Therefore, as the system is warmed up, λ_F and Λ become comparable in size, the ratio should approach k_B/e . This provides a simple explanation for the strong correlation between the magnitudes of $\sigma_{ij}^A(300\text{K})$ and $\alpha_{ij}^A(300\text{K})$ in all known topological magnetic systems.

Let us note that a similar approach, associating α_{ij}^A and Λ , explained why the magnitude of the anomalous Nernst effect (S_{ij}^A) in a given magnet anti-correlates with the mean-free-path¹³, while the ordinary Nernst effect correlates with the mean-free-path²⁶. In both cases, the driving idea is simple. The intrinsic anomalous α_{ij}^A (like the intrinsic anomalous σ_{ij}^A) should not depend on the mean-free-path, but on the average Berry curvature. In contrast, semiclassical α_{ij} (like semiclassical σ_{ij}) scale with the inverse of the square of the mean-free-path²⁶. Note also that the large anomalous thermoelectric response of Co_2MnGa is demystified by this approach. The room temperature α_{xy}^A of $3 \text{ AK}^{-1}\text{m}^{-1}$ is large compared to other topological magnets with lower AHE. Interestingly, BCC iron, whose room-temperature AHE is only slightly lower ($\simeq 1000 \Omega^{-1}\text{cm}^{-1}$ ^{16,27} has a room-temperature α_{xy}^A as large as $2 \text{ AK}^{-1}\text{m}^{-1}$. As the room-temperature S_{xy}^A is 20 times larger in Co_2MnGa than in Fe, it is partly because of its larger room-temperature resistivity ($125 \mu\Omega\text{cm}$ in Co_2MnGa compared to $10 \mu\Omega\text{cm}$ in Fe).

In summary, we studied the anomalous off-diagonal coefficients of Co_2MnGa and checked the validity of the anomalous transverse Wiedemann-Franz law in the whole temperature range. This confirms that the anomalous transverse response is fundamentally a Fermi surface property²⁸. We quantified α_{xy}^A and found that in all

known topological magnets its magnitude at room temperature has a universal relation with the size of the anomalous Hall conductivity and proposed an explanation for this observation.

Acknowledgements- This work was supported by the National Science Foundation of China (Grants No. 51861135104 and No. 11574097), by Agence Nationale de la Recherche (ANR-18-CE92-0020-01) in France, by CREST(JPMJCR18T3), Japan Science and Technology Agency, by Grants-in-Aids for Scientific Research on Innovative Areas (15H05882 and 15H05883) from the Min-

istry of Education, Culture, Sports, Science, and Technology of Japan, and by Grants-in-Aid for Scientific Research (19H00650) from the Japanese Society for the Promotion of Science (JSPS). Z. Z. was supported by the 1000 Youth Talents Plan and K. B. was supported by China High-end foreign expert program. L. X. acknowledges a PhD scholarship by the China Scholarship Council(CSC).

* zengwei.zhu@hust.edu.cn

* kamran.behnia@espci.fr

-
- [1] Nagaosa, N., Sinova, J., Onoda, S., MacDonald, A. H. & Ong, N. P. Anomalous hall effect. *Rev. Mod. Phys.* **82**, 1539–1592 (2010).
 - [2] Xiao, D., Chang, M.-C. & Niu, Q. Berry phase effects on electronic properties. *Rev. Mod. Phys.* **82**, 1959–2007 (2010).
 - [3] Nakatsuji, S., Kiyohara, N. & Higo, T. Large anomalous hall effect in a non-collinear antiferromagnet at room temperature. *Nature* **527**, 212 (2015).
 - [4] Xiao, D., Yao, Y., Fang, Z. & Niu, Q. Berry-phase effect in anomalous thermoelectric transport. *Phys. Rev. Lett.* **97**, 026603 (2006).
 - [5] Onoda, S., Sugimoto, N. & Nagaosa, N. Quantum transport theory of anomalous electric, thermoelectric, and thermal hall effects in ferromagnets. *Phys. Rev. B* **77**, 165103 (2008).
 - [6] Li, X. *et al.* Anomalous nernst and righi-leduc effects in Mn_3Sn : Berry curvature and entropy flow. *Phys. Rev. Lett.* **119**, 056601 (2017).
 - [7] Ikhlas, M. *et al.* Large anomalous nernst effect at room temperature in a chiral antiferromagnet. *Nat. Phys.* **13**, 1085–1090 (2017).
 - [8] Sakai, A. *et al.* Giant anomalous nernst effect and quantum-critical scaling in a ferromagnetic semimetal. *Nat. Phys.* **14**, 1119 (2018).
 - [9] Guin, S. N. *et al.* Anomalous Nernst effect beyond the magnetization scaling relation in the ferromagnetic Heusler compound Co_2MnGa . *NPG Asia Mater.* **11**, 16 (2019).
 - [10] Xu, L. *et al.* Finite-temperature violation of the anomalous transverse wiedemann-franz law in absence of inelastic scattering. *arXiv:1812.04339* (2018).
 - [11] Sugii, K. *et al.* Anomalous thermal hall effect in the topological antiferromagnetic state. *arXiv:1902.06601* (2019).
 - [12] Wuttke, C. *et al.* Berry curvature unravelled by the anomalous nernst effect in mn_3Ge . *Phys. Rev. B* **100**, 085111 (2019).
 - [13] Ding, L. *et al.* Intrinsic anomalous nernst effect amplified by disorder in a half-metallic semimetal. *Phys. Rev. X* **9**, 041061 (2019).
 - [14] Park, G.-H. *et al.* Thickness dependence of the anomalous nernst effect and the mott relation of weyl-semimetal Co_2MnGa thin films. *arXiv:1909.10168* (2019).
 - [15] Belopolski, I. *et al.* Discovery of topological Weyl fermion lines and drumhead surface states in a room temperature magnet. *Science* **365**, 1278–1281 (2019).
 - [16] Webster, P. J. Magnetic and chemical order in heusler alloys containing cobalt and manganese. *J. Phys. Chem. Solids* **32**, 1221–1231 (1971).
 - [17] Pechan, M. J., Yu, C., Carr, D. & Palmström, C. J. Remarkable strain-induced magnetic anisotropy in epitaxial Co_2MnGa (001) films. *J. Magn. Magn. Mater.* **286**, 340–345 (2005).
 - [18] Sato, T. *et al.* Large negative anisotropic magnetoresistance in Co_2MnGa heusler alloy epitaxial thin films. *Appl. Phys. Lett.* **113**, 112407 (2018).
 - [19] Manna, K. *et al.* From colossal to zero: controlling the anomalous hall effect in magnetic heusler compounds via berry curvature design. *Phys. Rev. X* **8**, 041045 (2018).
 - [20] Markou, A. *et al.* Thickness dependence of the anomalous Hall effect in thin films of the topological semimetal Co_2MnGa . *Phys. Rev. B* **100**, 54422 (2019).
 - [21] Reichlova, H. *et al.* Large anomalous nernst effect in thin films of the weyl semimetal Co_2MnGa . *Appl. Phys. Lett.* **113**, 212405 (2018).
 - [22] *See the supplemental material*.
 - [23] Onose, Y., Shiomi, Y. & Tokura, Y. Lorenz number determination of the dissipationless nature of the anomalous hall effect in itinerant ferromagnets. *Phys. Rev. Lett.* **100**, 016601 (2008).
 - [24] Miyasato, T. *et al.* Crossover behavior of the anomalous hall effect and anomalous nernst effect in itinerant ferromagnets. *Phys. Rev. Lett.* **99**, 086602 (2007).
 - [25] Nakayama, H. *et al.* Mechanism of strong enhancement of anomalous nernst effect in Fe by Ga substitution. *Phys. Rev. Materials* **3**, 114412 (2019).
 - [26] Behnia, K. & Aubin, H. Nernst effect in metals and superconductors: a review of concepts and experiments. *Rep. Prog. Phys.* **79**, 046502 (2016).
 - [27] Dheer, P. N. Galvanomagnetic effects in iron whiskers. *Phys. Rev.* **156**, 637–644 (1967).
 - [28] Haldane, F. D. M. Berry curvature on the fermi surface: Anomalous hall effect as a topological fermi-liquid property. *Phys. Rev. Lett.* **93**, 206602 (2004).
 - [29] Behnia, K. *Fundamentals of thermoelectricity* (Oxford University Press, 2015).
 - [30] Bergman, D. L. & Oganessian, V. Theory of dissipationless nernst effects. *Phys. Rev. Lett.* **104**, 066601 (2010).
 - [31] Zhang, C., Tewari, S., Yakovenko, V. M. & Das Sarma, S. Anomalous nernst effect from a chiral d -density-wave state in underdoped cuprate superconductors. *Phys. Rev. B* **78**, 174508 (2008).

Supplemental Material for "Anomalous transverse response of Co₂MnGa and universality of the room-temperature $\alpha_{ij}^A/\sigma_{ij}^A$ ratio across topological magnets"

S1. SAMPLE PREPARATION AND MEASUREMENTS

The single crystal Co₂MnGa were prepared by the Czochralski method⁸. The resistivity and Hall measurements were performed in a commercial measurement system (PPMS, Quantum Design) using the standard four-probe method with a pair of current source (Keithley 6221) and DC-Nanovoltmeter (Keithley 2182)¹⁰. The thermal gradient was measured by Type-E thermocouple¹⁰ in PPMS with high vacuum environment. The Nernst (Seebeck) voltage was detected by a DC-Nanovoltmeter separately. For thermal Hall effect measurements, we set $\mu_0 H$ at ± 1 T at different temperatures to get the anomalous thermal Hall conductivity. We also measured the transverse thermal conductivity with the function of field at some selected temperatures to get the normal part of thermal Hall effect. We used those convention in the main text (See Fig.1) to determine the sign for the transverse signal (Hall, Nernst and Righi-Leduc).

S2. CARRIER DENSITY AND MOBILITY

In the low temperature (2 K), carrier density n is $\approx 2.8 \times 10^{21} \text{ cm}^{-3}$, using the single-band model ($n = 1/eR_H$, where R_H is the Hall coefficient), along with the longitudinal resistivity $\rho_{xx} = 5.8 \times 10^{-7} \Omega\text{m}$, the carrier mobility results $\mu = 1/ne\rho \approx 38 \text{ cm}^2\text{V}^{-1}\text{s}^{-1}$. Fig.S2 shows the temperature evolution of Hall effect and thermal Hall effect. As it's depicted in Fig.S2a), the slope of ordinal Hall effect decrease a lot while increasing the temperature. We notes that it seems like the sign would change at a higher temperature.

S3. THE TWO COMPONENTS OF α_{ij}^A

The charge density current in a solid depends on both the electric field \mathbf{E} and the thermal gradient ∇T ²⁹:

$$\mathbf{J}_e = \sigma \mathbf{E} - \bar{\alpha} \nabla T \quad (\text{S1})$$

In absence of charge current, one has : $\mathbf{J}_e = 0$ and therefore $\sigma \mathbf{E} - \bar{\alpha} \nabla T = 0$. Since $S_{ij} = E_i / \nabla_j T$, one can write:

$$\bar{\alpha} = \sigma \vec{S} \quad (\text{S2})$$

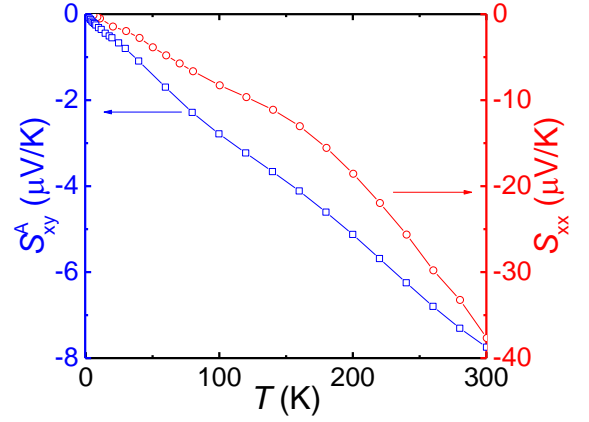


FIG. S1. **Anomalous Nernst coefficient and the Seebeck coefficient as a function of temperature:** The anomalous Nernst coefficient S^A_{xy} extracted from the field dependence of the Nernst effect at different temperatures. It attains $-7.8 \mu\text{V/K}$ at room temperature. The temperature dependence of the Seebeck coefficient is also shown.

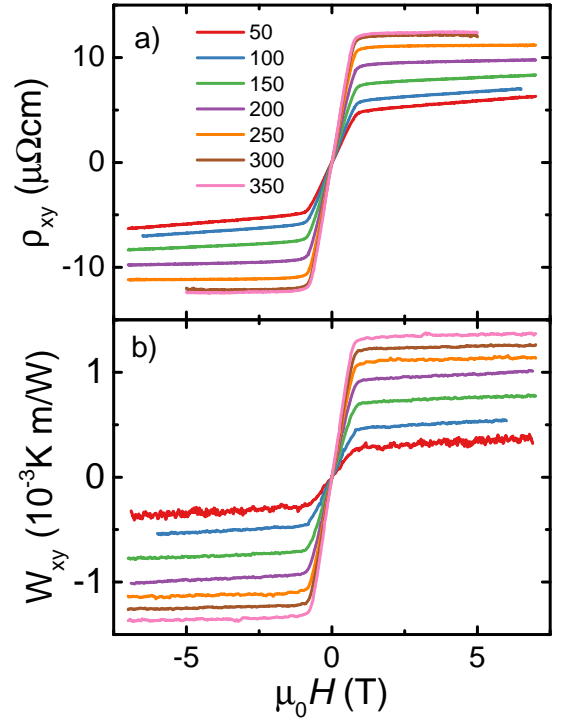


FIG. S2. The raw data: Temperature dependence of Hall resistivity (a)) and thermal Hall resistivity (b)) .

Eq.2 in the matrix form becomes:

$$\begin{pmatrix} \alpha_{xx} & \alpha_{xy} \\ \alpha_{yx} & \alpha_{yy} \end{pmatrix} = \begin{pmatrix} \sigma_{xx} & \sigma_{xy} \\ \sigma_{yx} & \sigma_{yy} \end{pmatrix} \begin{pmatrix} S_{xx} & S_{xy} \\ S_{yx} & S_{yy} \end{pmatrix} \\ = \begin{pmatrix} \sigma_{xx}S_{xx} + \sigma_{xy}S_{yx} & \sigma_{xx}S_{xy} + \sigma_{xy}S_{yy} \\ \sigma_{yx}S_{xx} + \sigma_{yy}S_{yx} & \sigma_{yx}S_{xy} + \sigma_{yy}S_{yy} \end{pmatrix}$$

As a consequence:

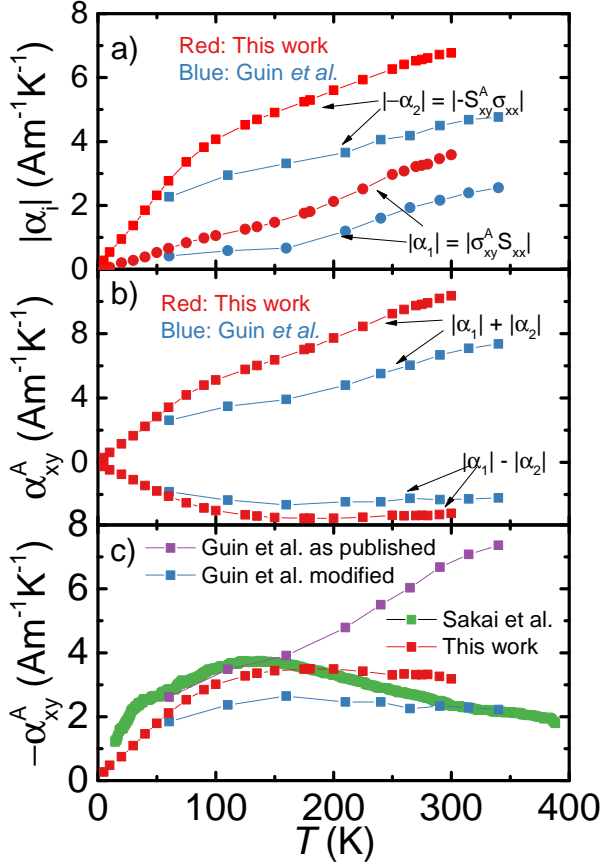


FIG. S3. **Two components of α_{xy}^A and the consistency**
a) Data by Guin *et al.* (blue)⁹ and this work (red) for the two components of α_{xy}^A in Eq.S3. $\alpha_1 = \sigma_{xy}^A S_{xx}$ and $\alpha_2 = -S_{xy}^A \sigma_{xx}$.
b) The sum and the difference of the two terms. Guin *et al.*⁹ added the two components, while the correct procedure is to subtract them. We note that the S_{xy}^A is positive in Guin *et al.* but negative here as a matter of convention.
c) α_{xy}^A of Co₂MnGa according to Guin *et al.* (modified), Sakai *et al.* and the present data. An overall consistency can be observed after correcting the mistake and assuming an opposite convention.

$$\alpha_{xy} = \sigma_{xx} S_{xy} + \sigma_{xy} S_{yy} \quad (S3)$$

This leads to the following expression between α_{xy} and experimentally measurable quantities:

$$\alpha_{xy} = \frac{\rho_{yy} S_{xy} - \rho_{xy} S_{yy}}{\rho_{xx} \rho_{yy} - \rho_{xy} \rho_{yx}} \quad (S4)$$

Two different conventions for defining S_{xy} have been used: $S_{xy} = E_x / \nabla_y T$ or $S_{xy} = E_x / -\nabla_y T$. The choice of convention for S_{xy} does not matter by itself. However, it can lead to mistakes on determining the magnitude of α_{xy} .

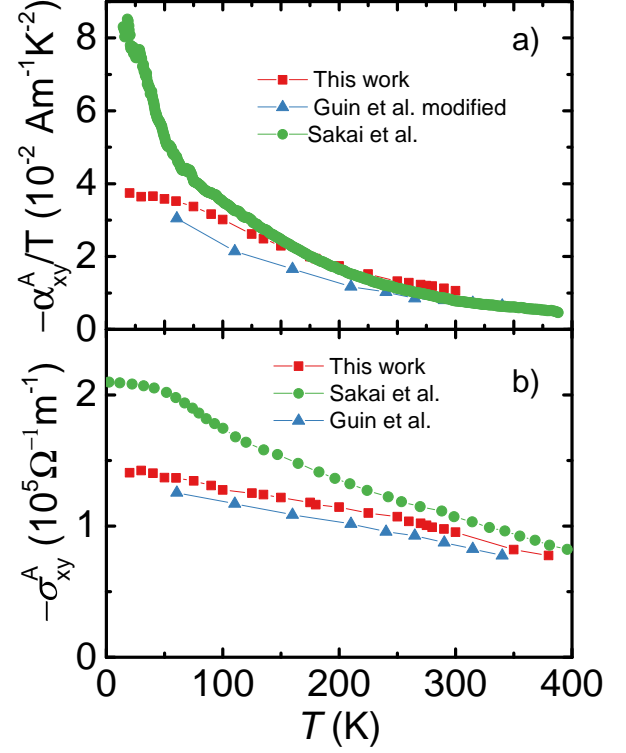


FIG. S4. **Comparison of α_{xy}^A/T and σ_{xy}^A reported in Co₂MnGa** a) α_{xy}^A/T according to Guin *et al.* (with opposite sign), Sakai *et al.* and this work. At low temperature the slope of α_{xy}^A/T is unambiguously found to be close to $-0.037 \text{ AK}^{-2} \text{ m}^{-1}$ in our data. The slope in the data reported by Sakai *et al.* is more ambiguous, but not very different. b) The temperature dependence of σ_{xy}^A according to the three different groups. The data by Sakai *et al.* is comparable to ours at room temperature, but slightly larger at low temperatures. The difference is attributable to a small change in the stoichiometry.

S4. α_{xy}^A AND σ_{xy}^A ACCORDING TO DIFFERENT GROUPS

Guin *et al.*⁹ report that α_{xy}^A in Co₂MnGa is as large as $7 \text{ AK}^{-1} \text{ m}^{-1}$. This is more than twice larger than what we or Sakai *et al.* find. The reason behind this discrepancy appears to be a simple mistake. They have apparently added instead of subtracting the two components of α_{xy}^A in the right side of Eq.S3. As seen in Fig.S3, the two components, namely $-\sigma_{xx} S_{xy}^A$ and $\sigma_{xy}^A S_{yy}$ have comparable values. Therefore the correct sign of these two parts is crucial in setting α_{xy}^A . After rectifying their data (Fig.S3), one sees that the correct α_{xy}^A from their measurements is non-monotonous like what was found by us and by Sakai *et al.* (Fig.S3c). The room-temperature magnitude of α_{xy}^A is close to $3 \text{ AK}^{-1} \text{ m}^{-1}$ in the three sets of data.

Thus, the magnitude of room-temperature α_{xy}^A and

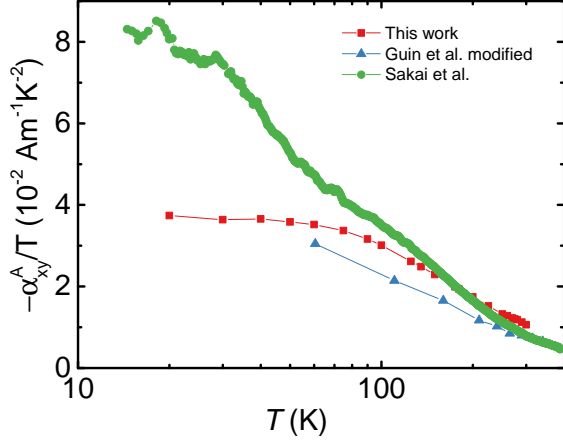


FIG. S5. **Logarithmic T dependence and quantum criticality-** In a semi-log plot, α_{xy}/T is indeed linear in $-\ln(T)$ in a finite temperature window, attributed to quantum criticality⁸. In the zero-temperature limit, α_{xy}/T saturates to a finite value.

σ_{xy}^A in Co_2MnGa appears to be known beyond reasonable doubt. On the other hand, as one can see in Fig.S4, in the low -temperature limit, the data by Sakai *et al.* indicates a non-monotonous σ_{xy}^A . The magnitude of α_{xy}/T in the zero-temperature limit according to their data is not very different from ours.

By plotting α_{xy}/T as a function of $\ln(T)$ (Fig.S5), one can see how the two sets of data compare with each other. According to Sakai *et al.*⁸, α_{xy}/T is almost linear in $\ln(T)$ between 20 K and 200 K. A crossover to a constant behavior from $\ln T$ dependence appears below 20 K. In our data the temperature window in which α_{xy}/T is linear in $\ln(T)$ is restricted to a high-temperature range above 100 K and the saturation to a constant value below 100 K is very clear. The difference in α_{xy}/T seen in the two sets of data may be ascribed to a small change in the stoichiometry and a slight shift in the Fermi energy. Future studies will tell if there is a critical doping at which the α_{xy}/T remains linear in $\ln(T)$ down to the lowest measured temperature as expected in a quantum-critical scenario.

S5. FERMI-SEA AND FERMI-SURFACE EXPRESSIONS FOR ANOMALOUS TRANSVERSE COEFFICIENTS

Xiao and co-workers wrote the following expression for the anomalous off-diagonal thermoelectric conductiv-

ity:⁴:

$$\alpha_{xy}^A = \frac{e}{T\hbar} \int \frac{d^3k}{(2\pi)^3} \Omega^z(k) F(k) \quad (\text{S5})$$

Here, $F(k) = (\epsilon - \mu)f(k) + \frac{1}{\beta} \ln[1 + e^{-\beta(\epsilon - \mu)}]$, $\beta = 1/k_B T$, $f(k)$ is the Fermi-Dirac distribution and T is the temperature.

A variable change $(\epsilon - \mu) \rightarrow f(k)$ ^{30,31} can show that $F(k)$ can be expressed in terms of the entropy density function $s(k) = -f(k)\ln(f(k)) - (1 - f(k))\ln(1 - f(k))$.

$$\begin{aligned} F(k) &= (\epsilon - \mu)f(k) + k_B T \ln[1 + e^{-\beta(\epsilon - \mu)}] \\ &= k_B T \{ \beta(\epsilon - \mu)f(k) + \ln[1 + e^{-\beta(\epsilon - \mu)}] \} \\ &= k_B T \{ \ln\left(\frac{1}{f(k)} - 1\right)f(k) + \ln\left[1 + \frac{1}{1/f(k) - 1}\right] \} \\ &= k_B T \{ \ln\left(\frac{1 - f(k)}{f(k)}\right)f(k) + \ln\left[1 + \frac{f(k)}{1 - f(k)}\right] \} \\ &= k_B T \{ [\ln(1 - f(k)) - \ln(f(k))]f(k) - \ln(1 - f(k)) \} \\ &= k_B T \{ -f(k)\ln(f(k)) - (1 - f(k))\ln(1 - f(k)) \} \\ &= k_B T s(k) \end{aligned}$$

The anomalous thermoelectric conductivity becomes:

$$\alpha_{xy}^A = \frac{k_B e}{\hbar} \int \frac{d^3k}{(2\pi)^3} \Omega^z(k) s(k) \quad (\text{S6})$$

This expression, used in the main text, is a Fermi-sea expression. The connection to the Fermi-surface expression can be seen by taking the derivative of $s(k)$

$$\begin{aligned} \frac{\partial s}{\partial \epsilon} &= -(\ln(f(k)) + 1) \frac{\partial f}{\partial \epsilon} - (-\ln(1 - f(k)) - 1) \frac{\partial f}{\partial \epsilon} \\ &= (-\ln(f(k)) + \ln(1 - f(k))) \frac{\partial f}{\partial \epsilon} \\ &= \ln\left(\frac{1 - f(k)}{f(k)}\right) \frac{\partial f}{\partial \epsilon} \\ &= \frac{\partial f}{\partial \epsilon} \frac{(\epsilon - \mu)}{k_B T} \end{aligned} \quad (\text{S7})$$

As in the case of anomalous Hall effect, the pondering factor in the Fermi-surface expression, is the negative energy deviation of that in Fermi sea picture, f .